Ir-Catalyzed Selective Reduction of CO_2 to Methoxy or Formate Level with $HSiMe(OSiMe_3)_2$

Jefferson Guzmán,[a] Pilar García-Orduña,[a] Víctor Polo,*[b] Fernando J. Lahoz,[a] Luis A. Oro[a] and Francisco J. Fernández-Alvarez*[a]

The iridium(III) complex $[Ir(CF_3CO_2)(\kappa^2\text{-}NSi)_2]$ (**3**) (NSi = (4-methylpyridine-2-yloxy)dimethylsilyl) has proven to be an effective catalyst for the reduction of CO_2 with $HSiMe(OSiMe_3)_2$ under mild reaction conditions. ^1H NMR studies of the **3**-catalyzed reactions of CO_2 with $HSiMe(OSiMe_3)_2$ in C_6D_6 at 298 K evidenced that the selectivity of these reduction processes depends on the pressure of CO_2. Thus, using CO_2 (4 bar) the corresponding silylformate was selectively obtained, while reducing the pressure of CO_2 to 1 bar the methoxysilane $CH_3OSiMe(OSiMe_3)_2$ was selectively formed. A mechanism proposal based on NMR experiments and theoretical calculations at the DFT level shows that the concentration of CO_2 influences in the selectivity of the overall catalytic process.

Introduction

The catalytic hydrogenation of CO_2 could be considered as the simplest methodology for the chemical reduction of CO_2 to formate or methanol. However, the utilization of hydrogen as reductant for the transformation of CO_2 is not always feasible. That is due to the energy cost required to produce hydrogen at industrial scale as well as to kinetic and thermodynamic parameters of the catalytic CO_2 hydrogenation processes.[1] In this regard, it is worth mentioning that silicon-hydrides have proven to be efficient reagents for the reduction of CO_2 to formate, aldehyde, methanol or methane level.[2] Conversely, the high price of hydrosilanes and the poor atom economy of these reduction processes hamper their application as reductants at industrial scale. In this context, hydrosiloxanes which are obtained in large scale as side products of the silicone industry have emerged during the last recent years as a cheaper alternative to hydrosilanes.[3] Hence, the development of catalytic systems effective for the selective reduction of CO_2 based on hydrosiloxanes is of great interest.

Selectivity is one of the major challenges in the catalytic reduction of CO_2 with silicon-hydrides (Scheme 1).[2] The reason is that under the reaction conditions the silylformate obtained from the hydrosilylation of CO_2[4-13] could further react with the excess of reducing agent present in the medium to afford bis(silyl)acetals (Scheme 1).[14-18] Moreover, bis(silyl)acetals are highly reactive towards silicon-hydrides in presence of hydrosilylation catalysts and therefore their transformation into the corresponding methoxysilane and siloxane is also possible (Scheme 1).[19-21] Finally, some catalytic systems have been able to promote the transformation of methoxysilanes in methane by their reaction with silicon-hydrides (Scheme 1).[22-24]

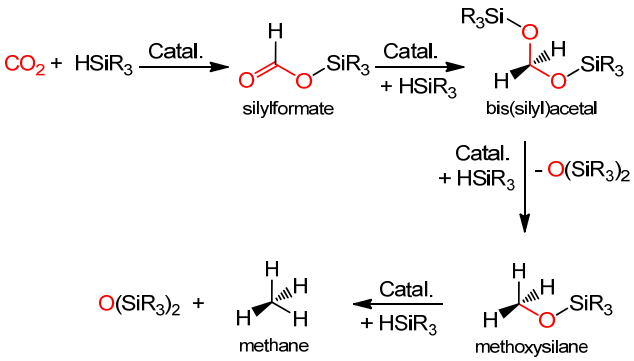

Scheme 1. Representation of the possible reaction products of the catalytic reduction of CO_2 with silicon-hydrides.

There are multiple reasons to use hydrosiloxanes instead of hydrosilanes, they are cheaper, stable and easy to handle.[3] As it has been stated above, some examples of transition metal-based catalysts active for the selective reduction of CO_2 to silylformates using hydrosiloxanes as reductants have been reported.[2] However, to the best of our knowledge the selective reduction of CO_2 to the methanol level using hydrosiloxanes as reductants has been scarcely explored.

The reduction of CO_2 with silicon-hydrides to give methoxysilanes was firstly achieved in 1989 using the iridium(I) complex [Ir(CN)(CO)(dppe)] (dppe = 1,2-bis(diphenylphosphane)ethane) as catalyst precursor and $HSiMe_3$ as reducing agent.[19] Since then only few examples of metal complexes[20] and *N*-heterocyclic carbenes with bulky substituents such as IMes[21] have been reported as selective catalysts for the reduction of CO_2 with silicon-hydrides to the corresponding methoxysilane.

In this context, our research team has reported that Ir-NSiN species (NSiN = bis(pyridine-2-yloxy)methylsilyl or bis(4-methylpyridine-2-yloxy)methylsilyl) are effective catalysts for the solvent-free hydrosilylation of CO_2[7,25] and for the dehydrogenative silylation of amines[26] and acetophenone derivatives.[27] In addition, these species have also promoted the insertion of CO_2 into the Si-N and Si-P bonds of silyl-amines[26] and silyl-phosphanes[28] to afford silylcarbamates or silylphosphanocarboxylates, respectively.

[a] *Departamento de Química Inorgánica – Instituto de Síntesis Química y Catálisis Homogénea (ISQCH). Universidad de Zaragoza. Facultad de Ciencias 50009, Zaragoza – Spain. E-mail: paco@unizar.es.*

[b] *Departamento de Química Física – Instituto de Biocomputación y Física de Sistemas complejos (BIFI) – Universidad de Zaragoza. Facultad de Ciencias 50009, Zaragoza – Spain. E-mail: vipolo@unizar.es*

Electronic Supplementary Information (ESI) available: [details of any supplementary information available should be included here]. See DOI: 10.1039/x0xx00000x

Ir-NSiN species catalyzed the reduction of CO_2 with silicon-hydrides to selectively afford silylformates.[25] Indeed, the corresponding bis(silyl)acetal and methoxysilane were only observed as minor reaction products under forcing reaction conditions. This behavior agrees with the low catalytic activity of Ir-NSiN species as catalysts for the reduction of silylesters (including silylformates) with silicon-hydrides.[29]

As consequence of our experience on the chemistry of Ir-NSiN species, our investigations focused on the search of iridium(III) catalysts bearing a more accessible active-site, which could facilitate the catalytic reduction of silylformates. Because of these studies, it has been found that iridium species of type Ir-(κ^2-NSi)$_2$ (NSi = (4-methylpyridine-2-yloxy)dimethylsilyl) are able to promote the selective reduction of CO_2 with $HSiMe(OSiMe_3)_2$ to give the corresponding methoxysilane $CH_3OSiMe(OSiMe_3)_2$.

Results and discussion

Preparation of the catalyst precursor. Treatment of commercially available 2-hydroxy-4-methyl-pyridine with $HSiMe_2Cl$ in presence of excess of freshly distilled NEt_3 affords the functionalized silane (4-methylpyridine-2-yloxy)dimethylsilane (**1**), which has been isolated as an amber liquid (Scheme 2). Compound **1** has been fully characterized by NMR spectroscopy (Figures S1-S3 and experimental) and used without further purifications. The ^{1}H NMR spectrum of **1** in C_6D_6 shows the resonance corresponding to the Si-H bond as a septet at δ 5.38 ppm, which is coupled ($^3J_{H\text{-}H}$ = 2.9 Hz) with a doublet resonance corresponding to the $SiMe_2$ protons that appears at δ 0.44 ppm. The ^{29}Si{^{1}H} NMR (C_6D_6) spectrum of **1** exhibits a singlet resonance at δ 2.9 ppm. Species **1** is highly reactive towards moisture, but it could be stored under argon for few weeks.

The reaction of two equivalents of **1** with half equivalent of [Ir(μ-Cl)(coe)$_2$]$_2$ (coe = *cis*-cyclooctene) in CH_2Cl_2 affords a white solid which has been characterized as the iridium(III) dinuclear species [Ir(μ-Cl)(κ^2-NSi)$_2$]$_2$ (**2**) (Scheme 2). Complex **2** has been fully characterized by means of elemental analysis, ^{1}H, ^{13}C and ^{29}Si NMR spectroscopy and by X-ray diffraction methods (Figure 1). ^{1}H NMR studies of the reaction of **1** with [Ir(μ-Cl)(coe)$_2$]$_2$ evidenced that the formation of **2** occurs via various unidentified Ir-H containing intermediate species[30] and is accompanied by evolution of free coe and of cyclooctane (coa) (Figure S4).

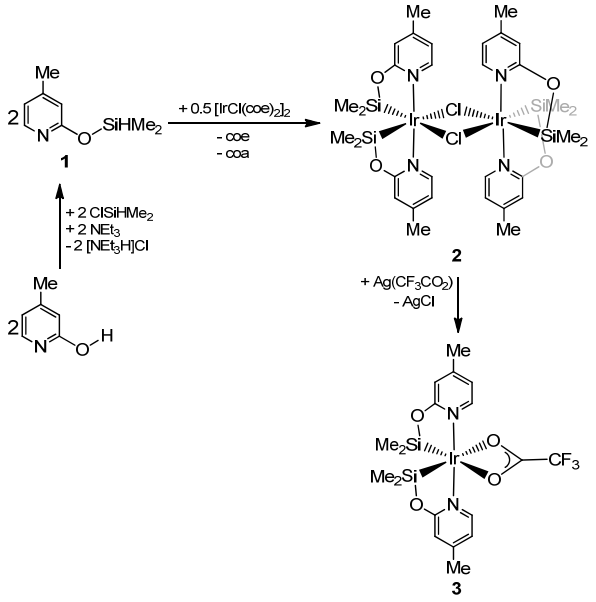

Scheme 2. Synthesis of [Ir(μ-Cl)(κ^2-NSi)$_2$]$_2$ (**2**) and [Ir(CF$_3$CO2)(κ^2-NSi)$_2$]$_2$ (**3**).

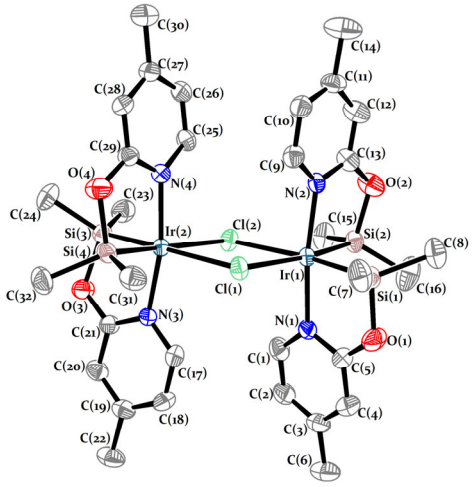

Figure 1. Molecular structure of complex **2**. Hydrogen atoms have been omitted for clarity. Selected bond lengths (Å) and angles (°) for **2**. Ir(1)-Cl(1), 2.6090(12); Ir(1)-Cl(2), 2.6283(12); Ir(1)-Si(1), 2.2634(14); Ir(1)-Si(2), 2.2695(14); Ir(1)-N(1), 2.078(4); Ir(1)-N(2), 2.074(4); Ir(2)-Cl(1), 2.6216(12); Ir(2)-Cl(2), 2.6118(12); Ir(2)-Si(3), 2.2552(14); Ir(2)-Si(4), 2.2747(14); Ir(2)-N(3), 2.069(4); Ir(2)-N(4), 2.073(4); Cl(1)-Ir(1)-Cl(2), 77.82(4); Cl(1)-Ir(2)-Cl(2), 77.89(4); Cl(1)-Ir(1)-Si(1), 94.74(5); Cl(1)-Ir(2)-Si(3), 173.70(5); Cl(1)-Ir(1)-Si(2), 172.07(5); Cl(1)-Ir(2)-Si(4), 93.04(5); Cl(1)-Ir(1)-N(1), 91.50(12); Cl(1)-Ir(2)-N(3), 95.84(12); Cl(1)-Ir(1)-N(2), 95.65(11); Cl(1)-Ir(2)-N(4), 93.70(11); N(1)-Ir(1)-N(2), 171.68(15); N(3)-Ir(2)-N(4), 169.51(15).

The solid-state structure of **2** evidenced its dinuclear nature and the bidentate coordination of the monoanionic NSi ligands (Figure 1). Metal atoms exhibit an octahedral geometry, with bridging chloride atoms and silicon atoms in equatorial plane, and apical positions fulfilled by nitrogen atoms. The iridium-silicon bond lengths in **2** (in the range 2.2552(14)-2.2747(14) Å) are shorter than those reported between the metal atom and the silicon atoms (located *trans* to bridging chlorides) in [(μ^2-Cl)$_2$Ir$_2$((SiMe$_2$CH$_2$-*o*-C$_6$H$_4$)$_2$P)$_2$((*o*-C$_6$H$_4$-CH$_2$SiMe$_2$)$_2$O)] (2.3050(12) and 2.3090(13) Å).[31] The pyridinic rings around the metallic centers in **2** are *trans* disposed one to each other, with similar Ir-N bond lengths (2.069(4)-2.078(4) Å). Deviations of

the N-Ir-N arrangement from the ideal value of 180° in **2** (N(1)-Ir(1)-N(2), 171.68(15)°; N(3)-Ir(2)-N(4), 169.51(15)°), may be related to the chelating bonding of the monoanionic NSi ligands through the formation of four Ir-Si-O-C-N metallacycles, with ring puckering parameters typical of $^5T_1$ / ^5E, ^2E, and $^2T_1$ conformations, respectively.[32]

The ^{1}H and ^{13}C NMR (CD_2Cl_2) spectra of **2** agrees with the highly symmetry of this species (Figures S5 and S8 and experimental). Thus, the ^{1}H NMR spectrum of **2** shows three resonances, two doublets at δ 8.61 and 6.13 ppm ($^3J_{H\text{-}H}$ = 6.1 Hz) and one singlet at δ 6.67 ppm, in the aromatic region, which allows to conclude that the four pyridinic rings are equivalent in solution. In addition, only two resonances were observed for the $SiMe_2$ groups in its ^{1}H and ^{13}C{^{1}H} NMR spectra. Furthermore, the ^{29}Si{^{1}H} NMR spectrum of **2** shows one singlet at δ 40.6 ppm for the four silicon atoms of the complex (Figure S8). This resonance is highly down-field shifted in comparison with that observed in the ^{29}Si{^{1}H} NMR spectra of the parent silane **1** (δ 2.9 ppm).

The reaction of **2** with two equivalents of silver trifluoroacetate in CH_2Cl_2 quantitatively gives the complex [Ir(CF_3CO_2)(κ^2-NSi)$_2$] (**3**), which has been isolated as a pale yellow solid in 88 % yield (Scheme 2).

Complex **3** crystallizes with two crystallographically independent but chemically identical molecules in the unit cell. Nitrogen atoms of pyridinic rings are *trans* disposed one to each other, with Ir-N bond lengths (in the range 2.049(3)-2.056(3) Å) shorter than those found in complex **2**, but similar to the mean value observed in the Cambridge Structural Database (mean value of Ir-N bond length between *trans* located pyridinic rings: 2.05(2) Å).[33] Relative spatial arrangements of aromatic rings are similar to those in complex **2**, while smaller deviations from the N-Ir-N ideal *trans*-disposition are found (N(1)-Ir(1)-N(2), 178.76(12)°; N(31)-Ir(31)-N(32), 176.46(11)°).

The chelating bonding of NSi ligands lead to the formation of two Ir-Si-O-C-N metallacycles in each molecule, with smaller ring puckering amplitudes than those reported in complex **2** ($^1T_2$, ^2E, ^2E and $^2T_1$ conformations, respectively).[32] Silicon-iridium bond lengths are close to those found in the parent compound and similar to the lower limit found in octahedral iridium complex (2.265-2.446 Å),[33] comparing well with that found in [IrH_2(SiClPh$_2$){xant(P^{i}Pr$_2$)$_2$}] complex 2.2654(11) Å.[34] Concerning the coordination of the trifluoroacetate, C-O bond lengths are statistically identical (1.247(5) and 1.249(5) Å, 1.246(4) and 1.253(4) Å) pointing out to the chelating bonding of the fragment. On the contrary, in one of the inequivalent molecules of **3**, the Ir-O bond lengths spread from 2.363(3) to 2.418(3) Å (in the other molecule 2.407(2) and 2.414(3) Å bond lengths are found). All these Ir-O distances are larger than the values usually found between iridium atom and acetate derivatives (around 2.30(1) Å in [(Phebox)Ir(mesityl)(OCCOCF$_3$)] (phebox=3,5-dimethylphenyl-2,6-bis-(oxazolinyl).[35] In fact, a 2.405(4) Å Ir-O distance *trans* to silicon atom has been found in [Ir(O_2CMe)H(biPSi)] (biPSi=κ-*P*,*P*,*Si*-Si(Me){(CH_2)$_3$PPh$_2$}$_2$), but the existence of a chemical bond with such a long distance has been argued.[36] These long Ir-O distances in **3** may be related to the strong *trans* influence of both silyl groups, weakening the coordination of the trifluoroacetate fragment, which could play a key role in the catalytic cycle of the hydrosilylation of CO_2 (see below).

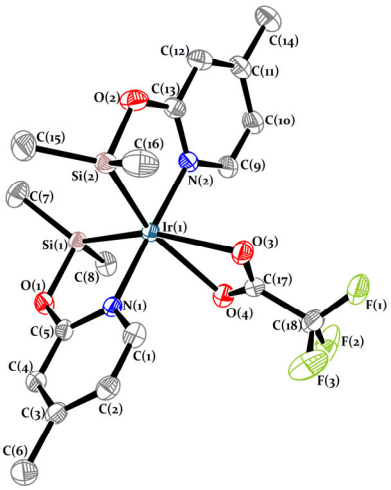

Figure 2. Molecular structure of complex **3**. Hydrogen atoms have been omitted for clarity. Selected bond lengths (Å) and angles (°) for **3**. Ir(1)-Si(1), 2.2645(10); Ir(1)-Si(2), 2.2505(11); Ir(1)-O(3), 2.363(3); Ir(1)-O(4), 2.418(3); Ir(1)-N(1), 2.052(3); Ir(1)-N(2), 2.056(3); Si(1)-Ir(1)-Si(2), 95.84(4); Si(1)-Ir(1)-O(3), 159.28(7); Si(1)-Ir(1)-O(4), 104.53(7); Si(1)-Ir(1)-N(1), 82.22(8); Si(1)-Ir(1)-N(2), 99.02(9); Si(2)-Ir(1)-O(3), 104.47(7); Si(2)-Ir(1)-O(4), 159.54(7); Si(2)-Ir(1)-N(1), 97.71(9); Si(2)-Ir(1)-N(2), 82.24(9).

The ^{1}H NMR spectrum of **3** shows three resonances in the aromatic region, two doublets at δ 8.04 and 6.64 ppm ($^3J_{H\text{-}H}$ = 6.2 Hz) and one singlet at δ 6.71 ppm, due to the CH protons of the pyridinic rings. In addition, it exhibits one singlet at δ 2.28 ppm assigned to the 4-methyl substituent, and two singlets at δ 0.42 and 0.38 corresponding to the $SiMe_2$ protons (Figure S9). The ^{29}Si{^{1}H} NMR spectra of **3** show one singlet at δ 39.7 ppm for the two silicon atoms of the complex (Figure S10). In addition, the ^{13}C{^{1}H} NMR spectra agree with the proposed structure (Figure S11).

Ir-(NSi)$_2$-catalyzed reduction of CO_2 with silicon-hydrides. ^{1}H NMR studies of the reaction of CO_2 (4.0 bar) with $HSiMe_2Ph$, $HSiMePh_2$ or $HSiMe(OSiMe_3)_2$ in C_6D_6 at 298 K in presence of **3** (5.0 mol%) evidenced that the reactions were selective to the formation of the corresponding silylformate (Table 1). The activity depends on the nature of the reductant. Thus, the reactions with $HSiMe(OSiMe_3)_2$ are faster than those carried out with $HSiMe_2Ph$ or $HSiMePh_2$ (Figure 3). The higher activity of $HSiMe(OSiMe_3)_2$ in comparison with $HSiMe_2Ph$ or $HSiMePh_2$ have been previously observed in Ir-NSiN catalyzed CO_2 hydrosilylation processes.[7a] Moreover, the less hindered Si-H bond in $HSiMe_2Ph$ is more reactive than that of $HSiMePh_2$ (Figure 3 and Table 1). Analogously to that reported for catalytic systems based on Ir-NSiN species,[7] it seems that the ancillary ligand plays a role on the mechanism of the catalytic process. Thus, when the chloride derivative **2** (5.0 mol%) was used as catalyst precursor of the reaction of CO_2 (4 bar) with $HSiMe(OSiMe_3)_2$, under the same reaction conditions that were used for **3**, only traces of the corresponding silylformate were observed after 24 h.

Table 1. Results from the ^{1}H NMR studies (C_6D_6) of the reaction of CO_2 with silicon-hydrides at 298 K in presence of **3**.

Silane	**3** mol%[a]	CO_2 bar	Formate[b] (%)	Methoxy[b,c] (%)	Time[d] (h)
$HSiMe(OSiMe_3)_2$	5	4	93.0	7.0	3.5
$HSiMe_2Ph$	5	4	>99.0	<1.0	14
$HSiMePh_2$	5	4	>99.0	<1.0	20
$HSiMe(OSiMe_3)_2$	5	3	55	45	4.5
$HSiMe_2Ph$	5	3	>99.0	<1.0	22
$HSiMePh_2$	5	3	99.0	1.0	36
$HSiMe(OSiMe_3)_2$	1	3	15	85	10
$HSiMe_2Ph$	1	3	>99.0	<1.0	30
$HSiMePh_2$	1	3	98.0	2.0	48

[a] % relative to Si-H, [b] Determined by ^{1}H NMR integration using hexamethylbenzene as internal standard. [c] The reaction products were characterized by comparison of ^{1}H and ^{29}Si{^{1}H} NMR spectra with reported data (see experimental section). [d] Time required for the full consumption of the starting silane or siloxane.

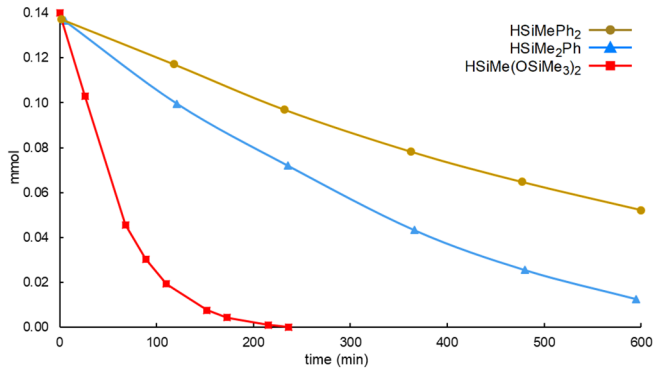

Figure 3. Representation of the consumption of the starting silicon-hydrides along the reaction of CO_2 (4.0 bar) with $HSiMe_2Ph$, $HSiMe(OSiMe_3)_2$ or $HSiMePh_2$ in C_6D_6 at 298K in presence of **3** (5.0 mol% relative to Si-H).

^{1}H NMR studies of the **3**-catalyzed reactions of CO_2 with the above-mentioned silicon compounds reducing the CO_2 pressure from 4 to 3 bar show a decrease of the reaction rate (Table 1). Under these conditions no changes in selectivity were observed when $HSiMe_2Ph$ or $HSiMePh_2$ were used as reductants. However, in the case of the reactions with $HSiMe(OSiMe_3)_2$ a clear change on the selectivity to the formation of methoxysilane (45%) was observed. Moreover, reducing the catalyst loading to 1.0 mol% and the CO_2 pressure to 3 bar showed, as it should be expected, a decrease of the activity being necessary 30, 48 and 10 h to achieve the full conversion of $HSiMe_2Ph$, $HSiMePh_2$ and $HSiMe(OSiMe_3)_2$, respectively (Table 1). Under these conditions the reactions with $HSiMe_2Ph$ and $HSiMePh_2$ maintain the selectivity to the formation of silylformate. However, in the case of the reactions with $HSiMe(OSiMe_3)_2$ an unexpected change of selectivity to the formation of $CH_3OSiMe(OSiMe_3)_2$ (85%) was observed (Table 1). ^{1}H NMR studies of the **3**-catalyzed (1.0 mol%) reaction of CO_2 (3.0 bar) with $HSiMe(OSiMe_3)_2$ show that at the beginning of the reaction, when the concentration of hydrosiloxane is higher than at the last stages, the silylformate is easily transformed into methoxysilane. Moreover, the resonances corresponding to the corresponding bis(silyl)acetal intermediate (Scheme 1) were barely observed. So, it is reasonable to assume that under the reaction conditions the reduction of bis(silyl)acetal to methoxysilane is faster than the NMR time scale.

A comparison of the catalytic performance of **3** and the previously reported complex $[IrH(CF_3CO_2)(NSiN)(coe)]$[7a] as catalysts for CO_2 hydrosilylation with $HSiMe(OSiMe_3)_2$ shows that complex **3** is more active than $[IrH(CF_3CO_2)(NSiN)(coe)]$ (Figure 4). The higher catalytic activity of **3** could be related to the fact that the two active sites are in *trans* position to a silyl group.

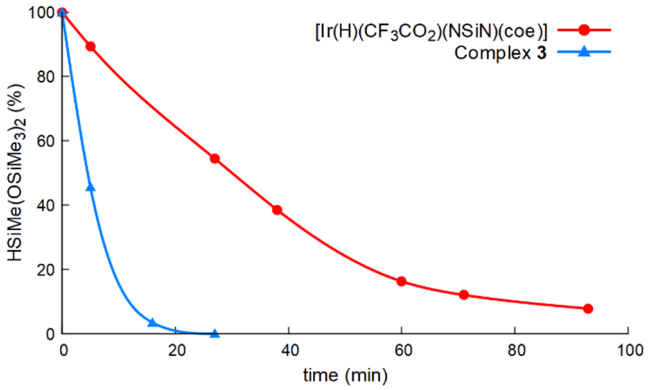

Figure 4. Representation of the consumption of the starting siloxane from the reaction of CO_2 (3 bar) with $HSiMe(OSiMe_3)_2$ in C_6D_6 at 328K in presence of catalytic amounts of complexes **3** or $[Ir(H)(CF_3CO_2)(NSiN)(coe)]$ (10.0 mol% relative to Si-H)

The above described outcomes suggest that a reduction of the CO_2 pressure should favour the selective formation of the corresponding methoxysiloxane. Indeed, ^{1}H NMR studies of the reaction of CO_2 (1.0 bar) with $HSiMe(OSiMe_3)_2$ in C_6D_6 at 298K in presence of catalytic amounts of complex **3** (1.0 mol%) evidenced the slow conversion of CO_2 into $CH_3OSiMe(OSiMe_3)_2$. ^{29}Si{^{1}H} NMR spectra evidenced that $CH_3OSiMe(OSiMe_3)_2$ and $O\{SiMe(OSiMe_3)_2\}_2$ are the major silicon containing reaction products (Figure S23).

Therefore, the selectivity of the Ir-$(NSi)_2$ catalyzed CO_2 hydrosilylation processes depends on the pressure of CO_2 (Scheme 3). This behavior is different to that observed for catalytic systems based on Ir-NSiN catalysts, which independently of the pressure of CO_2 were highly selective to the formation of the corresponding silylformate.[38] Thus, while the **3**-catalyzed reaction of CO_2 (4 bar, 298 K) with $HSiMe(OSiMe_3)_2$ selectively affords the corresponding silylformate, using CO_2 (1 bar, 298K) the corresponding methoxysilane (99%) was obtained after 16 h. The activity of **3**, as catalyst for the reduction of CO_2 to the methoxy level, is in

the range of activities reported for Re[20a] and Zn[20b] based catalysts.

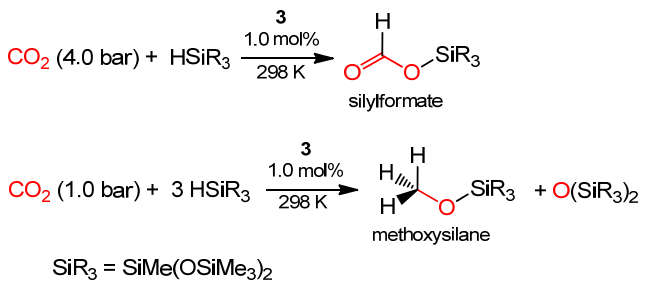

Scheme 3. **3**-Catalyzed reduction of CO_2 with $HSiMe(OSiMe_3)_2$.

^1H NMR spectra evidenced the presence of different intermediates depending on the reaction stage and on the CO_2 pressure. All the attempts to characterize any of these reaction intermediates have been unsuccessful. The ^1H NMR spectra of these catalytic reactions show the resonances due to $CF_3CH_2OSiMe(OSiMe_3)_2$,[7a] formed by reduction of the silylester $CF_3CO_2SiMe(OSiMe_3)_2$[7a]. In addition, the ^{19}F NMR spectra of these catalytic experiments at the end of the reactions show that $CF_3CH_2OSiMe(OSiMe_3)_2$ (δ -76.5 ppm, triplet, J_{H-F} = 8.7 Hz) is the major fluorinated species in solution together with one minor compound containing a $CF_3CH(O-)_2$ moiety (δ -84.6 ppm, doublet, J_{H-F} = 3.5 Hz) and traces of other unidentified species (Figure S28). These findings evidenced the reduction of the trifluoroacetate ancillary ligand.

The ^1H NMR studies of the **3**-catalyzed (1.0 mol%) reactions of CO_2 (1 and 3 bar) with $HSiMe(OSiMe_3)_2$ in C_6D_6 at 298 K evidenced the presence of a characteristic resonance at δ 10.39 ppm, which in the ^1H ^{13}C HSQC experiment correlates with a signal that appears at δ 174.5 ppm in the $^{13}C\{^1H\}$ NMR spectra (SI). Moreover, when the experiments were carried out with $^{13}CO_2$ (2.6 bar) this signal appeared as a doublet centered at δ 10.39 ppm ($^1J_{C-H}$ = 143.1 Hz). Therefore, these outcomes support the formation of an iridium-formate[37] species, which could be one of the intermediates of the **3**-catalyzed CO_2 hydrosilylation process.

In addition, these studies also show that the reaction rate depends on the CO_2 pressure. Thus, the **3**-catalyzed (1.0 mol%) reduction of CO_2 (3 bar) with $HSiMe(OSiMe_3)_2$ at 298K requires 10.8 h to achieve the full conversion of the starting $HSiMe(OSiMe_3)_2$ into a mixture of silylformate and methoxysilane, while using 1 bar of CO_2 under the same condition, 16 h were needed to complete the reaction (Figure S25).

Theoretical calculations. To shed light into the molecular mechanisms involved in the **3**-catalyzed CO_2 hydrosilylation, theoretical calculations at the DFT level have been carried out. The corresponding Gibbs free energy profiles for the reaction of complex **3**, labelled **A**, with $HSiMe_3$ and CO_2 are shown in Figures 5 and 6.

The calculations show that complex **A** can coordinate a molecule of silane to afford an iridium-σ-silane intermediate **B**. Examples of σ-coordination of silane to iridium centers have been previously experimentally observed.[39,40,41] The H-Si bond can be broken via metal ligand cooperation as shown by transition structure **TSBC**. The calculated energetic barrier for this step is 18.9 kcal mol^{-1}, leading to a hydride intermediate **C**. Ligand exchange of silyltrifluoroacetate by a molecule of CO_2 leads to intermediate **D**. In this context, it is worth mentioning that NMR spectra of the catalytic reactions evidenced the formation of CF_3CH_2O-$SiMe(OSiMe_3)_2$ along the reaction, which is obtained by reduction of the corresponding silylester. Therefore, the silylester $CF_3CO_2SiMe(OSiMe_3)_2$ is consumed during the reaction, which displaces the equilibrium **C/D** towards the formation of **D**. Intermediate **D** can be transformed into the formate derivative **E** by migratory insertion of the C=O bond into the Ir-hydride via transition state **TSDE** showing a relative energy of 9.7 kcal mol^{-1}. The formation of the formate **E** has been found to be thermodynamically favorable, exergonic by 14.3 kcal mol^{-1}. The stability of this intermediate agrees with the detection by ^1H and ^{13}C NMR spectroscopy of an iridium formate intermediate along the catalytic process. The formate derivative **E** can coordinate a molecule of silane yielding intermediate **F**. This species can evolve via transition state **TSFG** (like **TSBC**), to afford the observed silylformate and the Ir-hydride intermediate **G**. At this point, a bifurcation in the reaction path may occur.

Path i) follows a ligand exchange of silylformate by CO_2, leading to **D'** and closing the catalytic cycle.[42] Alternatively, following Path ii) the C=O bond of silylformate may undergo migratory insertion into the Ir-hydride as characterized by **TSGH**, leading to the silylacetal intermediate **H**. The silylacetal can react further if more silane molecules are present in the reaction media, as shown in Figure 6. Hence, coordination of one silane to the metal leads to intermediate **I** and via a σ-bond metathesis mechanism through the low energy transition state **TSIJ**, the bis(silyl)acetal intermediate **J** can be reached. Upon coordination of silane molecule to the metal, the experimentally obtained methyl silyl ether can be obtained via an S_N2 nucleophilic attack of the hydride to the carbon acting the siloxide as leaving group as shown by **TSJK**. The calculated energetic barrier for this step is 25.2 kcal mol^{-1}. The methyl silyl ether is released while the siloxide coordinates to the Ir(III) center leading to the iridium-σ-silane intermediate **K**, which presents a relative energy of -65.9 kcal mol^{-1}. Other mechanistic alternatives for transformation of **I** and **J** are shown in the ESI (Figure S31). The catalytic cycle is closed by formation of the bis(silyl)ether by σ-bond metathesis reaction between silane and the Ir-$OSiMe_3$ moiety and further coordination of a CO_2 molecule regenerating the active species **D''**. It should be noted that the oxidation state of the iridium atom remains invariable, Ir(III), along the catalytic process, like in Ir-NSiN catalyzed processes.[7a]

It should be noted that the calculated activation barrier towards the methoxysilane product is determined by the energetic difference between structures **J** and **TSJK** (25.2 kcal mol^{-1}). This value is excessively high for the current experimental conditions

and therefore no methoxysilane product should be observed when $HSiMe_3$ silane is employed, in agreement with the experimental results provided in Table 1. However, **TSJK** corresponds to a S_N2 nucleophilic attack of a hydride to the carbon atom of a bis(silyl)acetal where silyl groups are directly involved in the electronic rearrangements. Then, the nature of silyl substituents may play a key role in the activation energy of this step. DFT calculations on structures **J** and **TSJK** using $HSiMe(OMe)_2$ as a model of $HSiMe(OSiMe_3)_2$ (see SI) reveal a decrease in the activation energy for the methoxysilane pathway to 17.4 kcal mol^{-1}, making the pathway to the methoxysilane product affordable at the working conditions (Figure S32).

The experimental results indicate that silylformate is formed selectively under high CO_2 pressure while methoxysilane is the obtained product for low CO_2 pressure when silanes bearing siloxane groups were employed as reducing agents. The computational results reveal that the origin of the selectivity stands on intermediate **G**. Path i) leading to silylformate is followed by ligand exchange of silylformate by CO_2, therefore, a high concentration of CO_2 molecules in the reaction media is required. Otherwise, under low concentration of CO_2 molecules, path ii) leading to methoxysilane after addition of two silane molecules is followed.

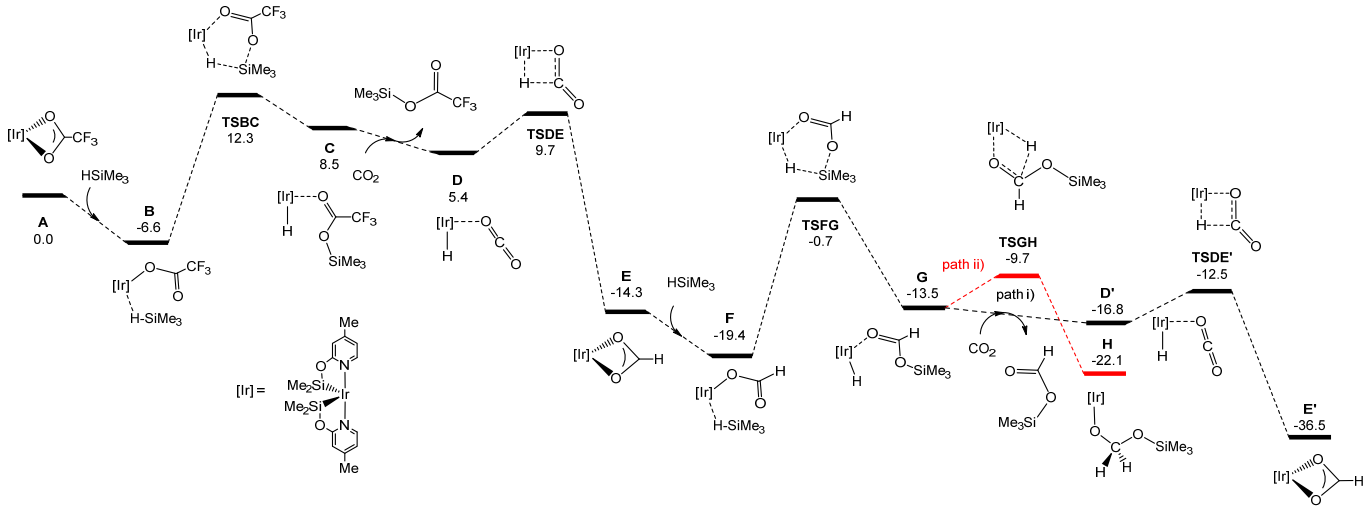

Figure 5. Gibbs free energy profile (in kcal mol^{-1}), relative to **A** and isolated molecules for the catalyst activation and silylformate formation

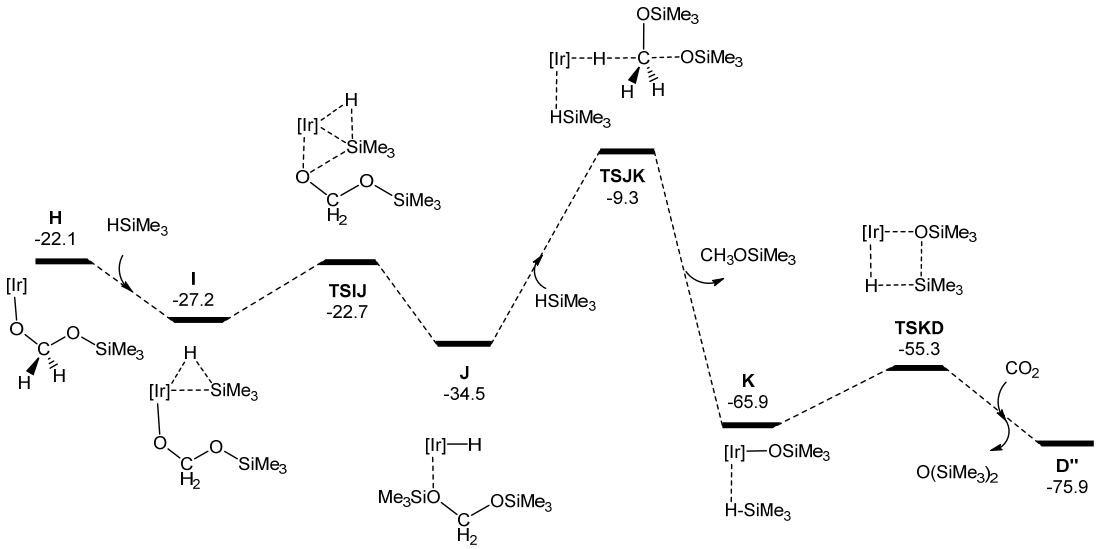

Figure 6. Gibbs free energy profile (in kcal mol^{-1}), relative to **A** and isolated molecules for methoxysilane formation with two equivalents of $HSiMe_3$.

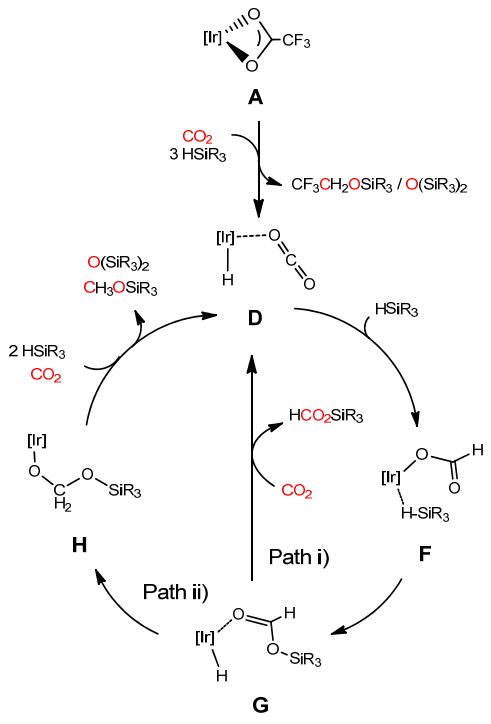

Figure 7. Proposed catalytic cycle for the **3**-catalyzed reduction of CO_2 with silanes.

A summary of the proposed mechanism for the catalytic cycle is presented in Figure 7. The catalyst precursor is activated by reaction of the trifluoroacetate ligand with silanes via metal-ligand heterolytic cleavage of the Si-H bond, forming the active hydride species **D**. Intermediate **D** evolves by migratory insertion of the coordinated CO_2 into the Ir-H bond and subsequent σ-coordination of a molecule of silane to give intermediate **F**. Again, the formate ligand can assist the cleavage the Si-H bond of a silane molecule to form one equivalent of silylformate and regenerate the hydride (**G**). From intermediate **G**, two different pathways arise. Path i) implies the substitution of silyformate by CO_2 to regenerate the active species **D** and closing the CO_2 hydrosilylation to silylformate catalytic cycle. Path ii) entails the insertion of the carboxylic moiety of the silylformate into the Ir-H bond to afford intermediate **H**, which in successive reactions with two equivalents of hydrosilane produces the corresponding methoxysilane and reaction with CO_2 produces $O(SiR_3)_2$ and regenerates the active species **D**. In agreement with the experimental and theoretical data, at high CO_2 pressure Path i) is favoured while at low (or zero) CO_2 pressure Path ii) is the productive one.

Experimental

General information. All reactions and manipulations were carried out under an argon atmosphere by using Schlenk-type techniques or in a Glovebox-MBraun UNIlab. Organic solvents were dried by standard procedures and distilled under argon prior to use or obtained oxygen- and water-free from a Solvent Purification System (Innovative Technologies). ^{1}H, ^{13}C, ^{29}Si and ^{19}F NMR spectra were obtained on a Bruker AV-300, AV-400 or AV-500 spectrometer using TMS as the internal reference in C_6D_6 as solvent. All chemical shifts (δ) are reported in ppm and coupling constants (*J*) are reported in Hz to apparent peak multiplications. ^{1}H-^{1}H-COSY, ^{13}C-APT, $^{1}H/^{13}C$ HSQC, $^{1}H/^{13}C$ HMBC and $^{1}H/^{29}Si$ HMBC sequences were used for helping in the assignments of the ^{1}H and $^{13}C\{^{1}H\}$ spectra.

Synthesis of 4-methylpyridine-2-yloxydimethylsilane (1). A THF solution (10 mL) of $HSiMe_2Cl$ (6.9 mL, 64.3 mmol) was slowly added to a solution of 2-hydroxy-4-methyl-pyridine (7.0 g, 64.1 mmol) and triethylamine (10.0 mL, 72.0 mmol) in THF (30 mL) at 273 K. After the addition the mixture was warmed to room temperature. The resulting solution was heated at 333 K for 20h. The white precipitate was filtered off and washed with hexane (3 x 10 mL). The filtrate and washing solutions were combined, dried *in vacuo*, and extracted with pentane (2 x 10 mL) to afford an amber liquid. Yield: 7.76 g (72 %). ^{1}H NMR plus HSQC ^{1}H–^{13}C (300 MHz, 298 K, C_6D_6): δ 7.93 (d, $^{3}J_{H\text{-}H}$ = 5.2 Hz, 1H, py-*6*), 6.47 (s, 1H, py-*3*), 6.30 (d, $^{3}J_{H\text{-}H}$ = 5.2, 1H, py-*5*), 5.38 (sp, *J* = 2.9 Hz, 1H, Si-*H*), 1.77 (s, 3H, C*H*$_3$-py), 0.44 (d, *J* = 2.9 Hz, 6H, SiMe). $^{13}C\{^{1}H\}$ APT plus HSQC ^{1}H–^{13}C (75 MHz, 298 K, C_6D_6): δ 163.5 (s, *C*$_2$-py), 150.4 (s, *C*$_4$-py), 147.2 (s, *C*$_6$-py), 118.6 (s, *C*$_5$-py), 112.9 (s, *C*$_3$-py), 20.5 (s, *C*H$_3$-py), -1.0 (s, $SiMe_2$). $^{29}Si\{^{1}H\}$ NMR (59.6 MHz, 298 K, C_6D_6): δ 2.9 (s).

Synthesis of [Ir(κ^2-NSi)$_2$(μ-Cl)]$_2$ (2). A CH_2Cl_2 solution (5 mL) of compound **1** (0.564 g, 3.39 mmol) was slowly added to a suspension of $[Ir(\mu\text{-}Cl)(coe)_2]_2$ (0.760 g, 0.848 mmol) in CH_2Cl_2 (15 mL) and the resulting mixture was stirred at room temperature for 6 h. The solvent was removed *in vacuo* and the residue washed with pentane cooled at 273 K (3 x 10 mL) to afford a white solid. Yield: 0.736 g (77%). Anal. Calcd. for $C_{32}H_{48}Cl_2IrN_4O_4Si_4$: C, 34.30; H, 4.32; N, 5.00. Found: C, 34.79; H, 4.57; N, 4.71. ^{1}H NMR plus HSQC ^{1}H–^{13}C (300 MHz, 298 K, CD_2Cl_2): δ 8.61 (d, $^{3}J_{H\text{-}H}$ 6.1 Hz, 2H, py-*6*), 6.67 (s, 2H, py-*3*), 6.13 (d, $^{3}J_{H\text{-}H}$ = 6.1 Hz, 2H, py-*5*), 2.26 (s, 6H, C*H*$_3$-py), 0.37 (s, 6H, SiMe), 0.21 (s, 6H, SiMe). $^{13}C\{^{1}H\}$ APT plus HSQC ^{1}H–^{13}C (75 MHz, 298 K, CD_2Cl_2): δ 169.3 (s, *C*$_2$-py), 151.0 (s, *C*$_4$-py), 150.1 (s, *C*$_6$-py), 117.9 (s, *C*$_5$-py), 111.6 (s, *C*$_3$-py), 21.2 (s, *C*H$_3$-py), 4.7 (s, SiMe), 3.3 (s, SiMe). $^{29}Si\{^{1}H\}$ NMR (HMBC ^{1}H–^{29}Si, 298 K, CD_2Cl_2): δ 40.6 (s). High Resolution Mass Spectrometry (ESI$^+$): calc. *m/z* = 525.1006; found *m/z* = 525.1039 (0.5 x (M^+-Cl)).

Synthesis of [Ir(κ^2-NSi)$_2$(CF$_3$CO$_2$)] (3). CH_2Cl_2 (15mL) was added to a light-protected Schlenk tube containing a mixture of complex **2** (0.400 g, 0.357 mmol) and silver trifluoroacetate (0.165 g, 0.724 mmol). The resulting suspension was stirred at room temperature for 6 h and filtered out through celite. The solvent was removed in vacuo and the residue extracted with pentane (3 x 10 mL) to afford a yellow solid. Yield 0.403 g (88 %). Anal. Calcd. for $C_{18}H_{24}F_3IrN_2O_4Si_2$: C, 33.90; H, 3.79; N, 4.39. Found: C, 33.24; H, 3.81; N, 4.26.^{1}H NMR plus HSQC ^{1}H–^{13}C (300 MHz, 298 K, CD_2Cl_2): δ 8.04 (d, $^{3}J_{H\text{-}H}$ = 6.2 Hz, 2H, py-*6*), 6.71 (s, 2H, py-*3*), 6.64 (d, $^{3}J_{H\text{-}H}$ = 6.2 Hz, 2H, py-*5*), 2.28 (s, 6H, C*H*$_3$-py), 0.42 (s, 6H, SiMe), 0.38 (s, 6H, SiMe). $^{13}C\{^{1}H\}$ NMR APT plus HSQC ^{1}H–^{13}C (75 MHz, 298 K, CD_2Cl_2): δ 168.9 (s, *C*$_2$-py), 152.6 (s, *C*$_4$-py), 147.5 (s, *C*$_6$-py), 118.8 (s, *C*$_5$-py), 112.2 (s, *C*$_3$-py), 21.3 (s, *C*H$_3$-py), 3.5 (s, SiMe), 2.4 (s, SiMe). $^{19}F\{^{1}H\}$ NMR (282 MHz, 298 K, CD_2Cl_2): δ -75.6 (C*F*$_3$CO$_2$). ^{29}Si NMR (HMBC ^{1}H–^{29}Si, 298 K,

CD_2Cl_2): δ 39.7 (s). High Resolution Mass Spectrometry (ESI^+): calc. *m/z* = 525.1006; found *m/z* = 525.1003 (M^+-CF_3CO_2).

Catalytic reactions at NMR scale with 5 mol% of catalyst relative to silicon. A Young cap NMR tube was filled with the catalyst precursor **3** (4.46 mg, 0.007 mmol), hexamethylbenzene (3.00 mg, 0.018 mmol), 0.14 mmol of the corresponding silane ($HSiMe_2Ph$, 21.5 µL; $HSiMePH_2$, 28 µL; and $HSiMe(OSiMe_3)_2$, 38.0 µL) and 0.5 mL of C_6D_6 was added. After that the solution was frozen and Argon was removed in vacuo, then the tube was pressurized with CO_2 (4 bar).

Catalytic reactions at NMR scale with 1 mol% of catalyst relative to silicon. A Young cap NMR tube was filled with the catalyst precursor **3** (2.68 mg, 0.042 mmol), hexamethylbenzene (3.00 mg, 0.018 mmol), 0.42 mmol of the corresponding silane ($HSiMe_2Ph$, 64.0 µL; $HSiMePH_2$, 84.0 µL; and $HSiMe(OSiMe_3)_2$, 114.0 µL) and 0.5 mL of C_6D_6. After that the solution was frozen and Argon was removed in vacuo, then the tube was pressurized with CO_2 (1 bar or 3 bar). When required the sample was heated at the desired temperature.

Selected data for $CH_3OSiMe(OSiMe_3)_2$. ^1H NMR plus HSQC ^1H–^{13}C (300MHz, C_6D_6, 298 K): δ 3.40 (s, 3H, CH_3OSi), 0.16 (s, 18H, $SiMe_3$), 0.12 (s, 3H, SiMe). $^{13}C\{^1H\}$ APT plus HSQC ^1H–^{13}C (75 MHz, C_6D_6, 298 K): δ 49.3 (s, CH_3OSi), 1.6 (s, $OSiMe_3$), -4.0 (s, SiMe). $^{29}Si\{^1H\}$ NMR plus ^1H–^{29}Si HMBC (60 MHz, C_6D_6, 298 K): δ 7.9 (s, $CH_3OSiMe(O\underline{Si}Me_3)_2$), -55.9 (s, $CH_3O\underline{Si}Me(OSiMe_3)_2$).

Selected data for $\{O(SiMe(OSiMe_3)_2\}_2$. ^1H NMR plus HSQC ^1H–^{13}C (300 MHz, C_6D_6, 298 K): δ 0.20 (br, SiMe and $OSiMe_3$). $^{13}C\{^1H\}$ APT plus HSQC ^1H–^{13}C (75 MHz, C_6D_6, 298 K): 1.7 (s, $OSiMe_3$), -2.4 (s, SiMe). $^{29}Si\{^1H\}$ NMR plus ^{29}Si–^1H HMBC (60 MHz, C_6D_6, 298 K): 7.5 (s, $OSiMe(O\underline{Si}Me_3)_2$), -65.5 (s, $\underline{Si}Me(OSiMe_3)_2$).

Structure determination of compounds 2 and 3. X-ray diffraction data were collected at 100(2)K with graphite-monochromated Mo Kα radiation (λ = 0.71073 Å) using narrow ω rotations (0.3°) on a Bruker APEX DUO (complex **2**) and Smart APEX (complex **3**) diffractometers. SAINT-PLUS[43] and SADABS[44] programs, included in APEX2 package were used to integrate and correct the intensities for absorption effects. The structures were solved by direct methods with SHELXS-2013[45] and refined by full-matrix least-squares refinement on F^2 with SHELXL-2014[46] included in WinGX.[47] CCDC 1858450-1858451 contains the supplementary crystallographic data for this paper. These data can be obtained free of charge from The Cambridge Crystallographic Data Centre via www.ccdc.cam.ac.uk/structures.

Crystal data compound 2. $C_{32}H_{48}Cl_2Ir_2N_4O_4Si_4$, *M* = 1120.40; colourless prism 0.065 x 0.075 x 0.200 mm^3; monoclinic *I*2/*a*, *a* = 17.8492(9), *b* = 10.6328(6), *c* = 43.5137(19) Å, *β*=96.227(2) °, *V* = 8209.6(7) $Å^3$; *Z* = 8; D_c = 1.813 g/cm^3; *μ* = 6.763 mm^{-1}; 43738/10107 reflections measured/unique (R_{int} = 0.0640), number of data/restraint /parameters 10107/0/445, $R_1(F^2)$ = 0.0325 (7539 reflections, $I > 2\sigma(I)$) and w$R(F^2)$ = 0.0773 (all data), final *GoF* = 0.898, largest difference peak: 1.388 $e.Å^{-3}$.

Crystal data compound 3. $2(C_{18}H_{24}F_3IrN_2O_4Si_2)\cdot 0.5(C_4H_{10}O)$, *M* = 1312.60; yellow prism 0.125 x 0.140 x 0.170 mm^3; triclinic $P\bar{1}$ *a* =11.4358(6), *b* = 13.0237(7), *c* = 17.6415(9) Å, *α* =90.2260(10), *β*=106.8990(10), γ=101.8860(10)°, *V* = 2454.4(2) $Å^3$; *Z* = 2; D_c = 1.776 g/cm^3; *μ* = 5.588 mm^{-1}; 47378/11954 reflections measured/unique (R_{int} = 0.0292), number of data/restraint /parameters 11954/0/586, $R_1(F^2)$ = 0.0276 (10240 reflections, $I > 2\sigma(I)$) and w$R(F^2)$ = 0.0625 (all data), final *GoF* = 1.036, largest difference peak: 1.272 $e.Å^{-3}$. Diethyl ether has been found to be disordered. Methylene carbon atom has been included in the model in two sets of positions and isotropically refined with 0.5 occupancy factor values.

Computational details. All DFT theoretical gas-phase calculations were carried out using the Gaussian program package.[48] The B3LYP method,[49] including the D3 dispersion correction scheme developed by Grimme[50] with Becke Johnson damping, has been used for both energies and gradient calculations. All atoms were treated with the def2-SVP basis set[51] together with the corresponding core potential for Iridium for geometry optimizations. Energies were further refined by single point calculations using the def2-TZVP basis set. The "ultrafine" grid was employed in all calculations. All reported energies are Gibbs free energies referred to a 1 M standard state at 328.15 K removing the contribution to the translational entropy, as indicated by Morokuma et al.[52] The nature of the stationary points was confirmed by analytical frequency analysis, and transition states were characterized by a single imaginary frequency corresponding to the expected motion of the atoms.

Conclusions

The iridium complex $[Ir(CF_3CO_2)(\kappa^2\text{-NSi})_2]$ (**3**) (NSi = (4-methylpyridine-2-yloxy)dimethylsilyl) has proven to be an effective catalyst for the reduction of CO_2 with $HSiMe(OSiMe_3)_2$ under mild reaction conditions. The nature of the silane influences the performance of the catalytic system, so $HSiMe(OSiMe_3)_2$ has found to be more active than $HSiMe_2Ph$ and $HSiMePh_2$. ^1H NMR studies of the **3**-catalyzed reactions of CO_2 with $HSiMe(OSiMe_3)_2$ in C_6D_6 at 298 K evidenced that the selectivity of these reduction processes depends on the pressure of CO_2, the concentration of hydrosiloxane, the catalyst loading and the temperature.

Thus, using a CO_2 pressure of 4 bar and a catalyst loading of 5.0 mol% the corresponding silylformate was selectively obtained. On the other hand, decreasing the CO_2 pressure and the catalyst loading produces a change on the selectivity. So, the **3**-catalyzed (1.0 mol%) reaction of CO_2 (1 bar) with $HSiMe(OSiMe_3)_2$ in C_6D_6 at 298 K affords selectively the corresponding methoxysiloxane $CH_3OSiMe(OSiMe_3)_2$.

In agreement with the experimental observations, a computational study for the reaction mechanisms leading to silylformate and methoxysilane products has been carried out. The calculations show that the **3**-catalyzed CO_2 reduction to silylformate is favoured to the **3**-catalyzed reduction of silylformate to methoxysilane process by 7.1 kcal mol^{-1}, if CO_2 molecules are abundant in the reaction media. These findings explain that at high CO_2 pressure (excess of CO_2) the corresponding silylformate is obtained while low CO_2 pressure (defect of CO_2) is required to selectively produce the corresponding methoxysilane.

Conflicts of interest

"There are no conflicts to declare".

Acknowledgements

Financial support from MINECO/FEDER project CTQ2015-67366-P and DGA/FSE group E07 is gratefully acknowledged. Dr. P. García-Orduña acknowledges CSIC, European Social Fund and Ministerio de Economía y Competitividad of Spain for a PTA contract. V.P. gratefully acknowledges the resources from the supercomputer "memento" and technical assistance provided by BIFI-ZCAM. Authors would like to acknowledge the use of Servicio General de Apoyo a la Investigación-SAI, Universidad de Zaragoza.

Notes and references

1 For recent reviews on catalytic hydrogenation of CO_2 see: (a) K. Sordakis, C. Tang, L. K. Vogt, H. Junge, P. J. Dyson, M. Beller, G. Laurenczy, *Chem. Rev.*, 2018, **118**, 372−433; (b) S. Kar, J. Kothandaraman, A. Goeppert, G. K. S. Prakash, *J. CO_2 Utilization*, 2018, **23**, 212-218; (c) H. Yang, C. Zhang, P. Gao, H. Wang, X. Li, L. Zhong, W. Wei, Y. Sun, *Catal. Sci. Technol.,* 2017, **7**, 4580-4598; (d) W. H. Bernskoetter, N. Hazari, *Acc. Chem. Res.*, 2017, **50**, 1049−1058; (e) J. Klankermayer, S. Wesselbaum, K. Beydoun, W. Leitner, *Angew .Chem. Int. Ed.*, 2016, **55**, 7296–7343; (f) W.-H. Wang, Y. Himeda, J. T. Muckerman, G. F. Manbeck, E. Fujita, *Chem. Rev.*, 2015, **115**, 12936−12973; (g) S. Saeidi, N. A. S. Amin, M. R. Rahimpour, *J. CO_2 Utilization*, 2014, **5**, 66–81; (h) Y.-N. Li, R. Ma, L.-N. He, Z.-F. Diao, *Catal. Sci. Technol.*, 2014, **4**, 1498–1512; (i) W. Wang, S. Wang, X. Ma, J. Gong, *Chem. Soc. Rev.*, 2011, **40**, 3703–3727; (j) P. G. Jessop, F. Joó, C.-C. Tai, *Coord. Chem. Rev.*, 2004, **248**, 2425–2442.

2 For recent reviews see: (a) F. J. Fernández-Alvarez, L. A. Oro, *ChemCatChem*, 2018, **10**, 4783-4796; (b) C. Chauvier, T. Cantat, *ACS Catal.*, 2017, **7**, 2107-2115; (c) F. J. Fernández-Alvarez, A. M. Aitani, L. A. Oro, *Catal. Sci. Technol.,* 2014, **4**, 611-624.

3 (a) D. Addis, S. Das, K. Junge, M. Beller, *Angew. Chem. Int. Ed.,* 2011, **50**, 6004-6011; (b) S. Chandrasekhar, C. R. Reddy, B. N. Babu, *J. Org. Chem.*, 2002, **67**, 9080–9082; (c) N. J. Lawrence, M. D. Drew, S. M. Bushell, *J. Chem. Soc., Perkin Trans. 1.*, 1999, 3381–3391.

4 For examples of Ru catalysts see: (a) P. Deglmann, E. Ember, P. Hofmann, S. Pitter, O. Walter, *Chem. Eur. J.*, 2007, **13**, 2864–2879; (b) A. Jansen, S. Pitter, *J. Mol. Catal. A. Chem.*, 2004, **217**, 41–45; (c) A. Jansen, H. Görls, S. Pitter, *Organometallics*, 2000, **19**, 135–138.

5 For examples of Co catalysts see: M. L. Scheuermann, S. P. Semproni, I. Pappas, P. J. Chirik, *Inorg. Chem.*, 2014, **53**, 9463–9465.

6 For examples of Rh catalysts see: S. Itagaki, K. Yamaguchi, N. Mizuno, *J. Mol. Catal. A. Chem.*, 2013, **366**, 347–352.

7 For examples of Ir catalysts see: (a) A. Julián, J. Guzmán, E. A: Jaseer, F. J. Fernández-Alvarez, R. Royo, V. Polo, P. García-Orduña, F. J. Lahoz, L. A. Oro, *Chem. Eur. J.,* 2017, **23**, 11898-11907; (b) A. Julián, E. A. Jaseer, K. Garcés, F. J. Fernández-Alvarez, P. García-Orduña, F. J. Lahoz, L. A. Oro, *Catal. Sci.Technol.*, 2016, **6**, 4410-4417; (c) R. Lalrempuia, M. Iglesias, V. Polo, P. J. Sanz Miguel, F. J. Fernández-Alvarez, J. J. Pérez-Torrente, L. A. Oro, *Angew. Chem. Int. Ed.*, 2012, **51**, 12824–12827.

8 For examples of Pd catalysts see: J. Takaya, N. Iwasawa, *J. Am. Chem. Soc.*, 2017, **139**, 6074-6077.

9 For examples of Pd catalysts see: P. Rios, J. Díez, J. López-Serrano, A. Rodriguez, S. Conejero, *Chem. Eur. J.*, 2016, **22**, 16791-16795.

10 For examples of Cu catalysts see: (a) K. Motokura, D. Kashiwame, A. Miyaji, T. Baba, *Org. Lett.*, 2012, **14**, 2642–2645; (b) K. Motokura, D. Kashiwame, N. Takahashi, A. Miyaji, T. Baba, *Chem. Eur. J.*, 2013, **19**, 10030–10037.

11 For examples of Ni catalysts see: L. González-Sebastián, M. Flores-Alamo, J. J. García, *Organometallics*, 2013, **32**, 7186−7194.

12 For examples of Zn catalysts see: (a) W. Sattler, G. Parkin, *J. Am. Chem. Soc.*, 2012, **134**, 17462−17465; (b) D. Specklin, C. Fliedel, C. Gourlaouen, J.-C. Bruyere, T. Aviles, C. Boudon, L. Ruhlmann, S. Dagorne, *Chem. Eur. J.*, 2017, **23**, 5509–5519.

13 For metal-free catalysts se: (a) K. Motokura, M. Naijo, S. Yamaguchi, A. Miyaji, T. Baba, *Chem. Lett.*, 2015, **44**, 1217-1219; (b) C. C. Chong, R. Kinjo, *Angew. Chem. Int. Ed.*, 2015, **54**, 12116-12120; (c) M.-A. Courtemanche, M.-A. Légaré, E. Rochette, F.-G. Fontaine, *ChemCommun.*, 2015, **51**, 6858-6861.

14 Y. Jing, O. Blacque, T. Fox, H. Berke, *J. Am. Chem. Soc.*, 2013, **135**, 7751-7760.

15 T. T. Metsänen, M. Oestreich, *Organometallics*, 2015, **34**, 543-546.

16 (a) P. Rios, N. Curado, J. López-Serrano, A. Rodriguez, *Chem. Commun*., 2016, **52**, 2114-2117; (b) P. Rios, A. Rodriguez, J. López-Serrano, *ACS Catal.*, 2016, **6**, 5715-5723.

17 F. A. LeBlanc, W. E. Piers, M. Parvez, *Angew. Chem. Int. Ed.*, 2014, **53**, 789-792.

18 N. Del Rio, M. Lopez-Reyes, A. Baceiredo, N. Saffon-Merceron, D. Lutters, T. Müller, T. Kato, *Angew. Chem. Int. Ed.*, 2017, **56**, 1365-1370.

19 T. C. Eisenschmid, R. Eisenberg, *Organometallics*, 1989, **8**, 1822-1824.

20 (a) D. S. Morris, C. Weetman, J. T. C. Wennmacher, M. Cokoja, M. Drees, F. E. Kühn, J. B. Love, *Catal. Sci. Technol.*, 2017, **7**, 2838-2845; (b) D. Specklin, F. Hild, C. Fliedel, C. Gourlaouen, L. F. Veiros, S. Dagorne, *Chem. Eur. J.* **2017**, *23*, 15908–15912.

21 S. N. Riduan, Y. Zhang, J. Y. Ying, *Angew. Chem. Int. Ed.*, 2009, **48**, 3322-3325.

22 (a) D. Mukherjee, D. F. Sauer, A. Zanardi, J. Okuda, *Chem. Eur. J.*, 2016, **22**, 7730-7733; (b) A. Berkefeld, W. E. Piers, M. Parvez, L. Castro, L. Maron, O. Eisenstein, *Chem. Sci.*, 2013, **4**, 2152-2162; (c) A. Berkefeld, W. E. Piers, M. Parvez, *J. Am. Chem. Soc.*, 2010, **132**, 10660-10661; (d) T. Matsuo, H. Kawaguchi, *J. Am. Chem. Soc.*, 2006, 128, 12362-12363.

23 (a) S. Park, D. Bézier, M. Brookhart, *J. Am. Chem. Soc.*, 2012, **134**, 11404-11407; (b) S. J. Mitton, L. Turculet, *Chem. Eur. J.*, 2012, **18**, 15258-15262; (c) M. Khandelwal, R. J. Wehmschulte, *Angew. Chem. Int. Ed.*, 2012, **51**, 7323-7326; (d) R. J. Wehmschulte, M. Saleh, D. R. Powell, *Organometallics*, 2013, **32**, 6812-6819.

24 T. Jurado-Vazquez, C. Ortiz-Cervantes, J. J. García, *J. Organomet. Chem.*, 2016, **823**, 8-13.

25 F. J. Fernández-Alvarez, R. Lalrempuia, Luis A. Oro, *Coord. Chem. Rev.*, 2017, **350**, 49-60.

26 A. Julián, V. Polo, E. A. Jaseer, F. J. Fernández-Alvarez, L. A. Oro, ChemCatChem, 2015, **7**, 3895 –3902.

27 K. Garcés, R. Lalrempuia, V. Polo, F. J. Fernández-Alvarez, P. García-Orduña, F. J. Lahoz, J. J. Pérez-Torrente, L. A. Oro, *Chem. Eur. J.*, 2016, **22**, 14717-14729.

28 A. Julián, V. Polo, F. J. Fernández-Alvarez, L. A. Oro, *Catal. Sci. Technol.*, 2017, **7**, 1372–1378.

29 A. Julián, K. Garcés, R. Lalrempuia, E. A. Jaseer, P. García-Orduña, F. J. Fernández-Alvarez, F. J. Lahoz, L. A. Oro, *ChemCatChem*, 2018, **10**, 1027 –1034.

30 The reaction of one equivalent of **1** with one equivalent of $[Ir(\mu\text{-}Cl)(coe)_2]_2$ in CH_2Cl_2 (or toluene) at 298K affords mixtures of complex **2** and others unidentified iridium complexes.
31 M. V. Corona-González, J. Zamora-Moreno, C. A. Cuevas-Chávez, E. Rufino-Felipe, E. Mothers-Martin, Y. Coppel, M. A. Muñoz-Hernández, L. Vendier, M. Flores-Alamo, M. Grellier, S. Sabo-Etienne, V. Montiel-Palma, *Dalton Trans*., 2017, **46**, 8827-8838.
32 D. Cremer, J. A. Pople, *J. Am. Chem. Soc.*, 1975, **97**, 1354–1358.
33 C. R Groom, I. J. Bruno, M. P. Lightfoot, S. C. Ward, *Acta Crystallogr*., 2016, **B72**, 171-179.
34 M. A. Esteruelas, M. Oliván, A. Vélez, *Inorg. Chem*., 2013, **52**, 12108-12119.
35 M. Zhou, S. I. Johnson, Y. Gao, T. J. Emge, R. J. Nielsen, W. A. Goddard, A. S. Goldman, *Organometallics*, 2015, **34**, 2879-2888.
36 E. Sola, A. García-Camprubí, J. L. Andrés, M. Martín, P. Plou, *J. Am. Chem. Soc.*, 2010, **132**, 9111–9121.
37 P. Kang, C. Cheng, Z. Chen, C. K. Schauer, T. J. Meyer, M. Brookhart, *J. Am. Chem. Soc.*, 2012, **134**, 5500-5503.
38 H. B. Oladipo, E. A. Jaseer, A. Julián, F. J. Fernández-Alvarez, S. Al-Khattaf, L. A. Oro, *J. CO_2 Utilization*, 2015, **12**, 21–26.
39 For examples of κ1-silane metal complexes, see: (a) J. Y. Corey, *Chem. Rev.*, 2016, **116**, 11291-11435; (b) J. Y. Corey, *Chem. Rev.*, 2011, **111**, 863-1071.
40 Examples of iridium-σ-silane complexes have been characterized by X-ray diffraction methods: J. Yang, P. S. White, C. K. Schauer, M. Brookhart, *Angew. Chem. Int. Ed.*, 2008, **47**, 4141–4143.
41 Iridium-σ-silane complexes have been proposed as intermediates in several catalytic processes, see: M. C. Lipke, A. L. Liberman-Martin, T. Don Tilley, *Angew. Chem. Int. Ed.*, 2017, **56**, 2260 – 2294.
42 D and D' are the same structures but energies are different because one turnover of the catalytic cycle has been completed.
43 SAINT+, version 6.01: Area-Detector Integration Software, Bruker AXS, Madison, WI, 2001
44 SADABS, Area Detector Absorption Correction Program, Bruker AXS, Madison, WI, 1996.
45 G. M. Sheldrick, *Acta Cryst.*, 1990, **A46**, 467-473.
46 G. M. Sheldrick, *Acta Cryst.*, 2008, **A64**, 112-122.
47 L. J. Farrugia, *J. Appl. Cryst.*, 2012, **45**, 849-854.
48 Gaussian 09, Revision D.01, full citation in the supporting information.
49 (a) C. Lee, W. Yang, R. G. Parr, *Phys. Rev. B*, 1988, **37**, 785–789; (b) A. D. Becke, *J. Chem. Phys.*, 1993, **98**, 1372–1377; (c) A. D. Becke, *J. Chem. Phys.*, 1993, **98**, 5648–5652.
50 S. Grimme, J. Antony, S. Ehrlich, H. Krieg, *J. Chem. Phys.*, 2010, **132**, 154104.
51 F. Weigend, R. Ahlrichs, *Phys. Chem. Chem. Phys.*, 2005, **7**, 3297–3305.
52 R. Tanaka, M. Yamashita, L. W. Chung, K. Morokuma, K. Nozaki, *Organometallics*, 2011, **30**, 6742–6750.